

Experimental validation of coupled heat, air and moisture transfer modeling in multilayer building components

M. Y. Ferroukhi¹ · K. Abahri² · R. Belarbi¹ · K. Limam¹ · A. Nouviaire¹

Received: 25 March 2015 / Accepted: 9 December 2015 / Published online: 17 December 2015
© Springer-Verlag Berlin Heidelberg 2015

Abstract The present paper lies to study the coupled heat, air and moisture transfer in multi-layer building materials. Concerning the modeling part, the interest is to predict the hygrothermal behavior, by developing a macroscopic model that incorporates simultaneously the diffusive, convective and conductive effects on the building elements. Heat transfer is considered in the strongly coupled situation where the mass and heat flux are temperature, vapor pressure and total pressure dependents. The model input parameters are evaluated experimentally through the development of various experimental prototypes in the laboratory. Thereafter, an experimental setup has been established in order to evaluate the hygrothermal process of several multilayer walls configurations. The experimental procedure consists to follow the temperature and relative humidity evolutions within the samples thickness, submitted to controlled and fixed boundary conditions. This procedure points out diverging conclusion between different testing materials combinations (e.g. red-brick and polystyrene). In fact, the hygrothermal behavior of the tested configurations is completely dependent on both materials selection and their thermophysical properties. Finally, comparison between numerical and experimental results showed good agreement with acceptable errors margins with an average of 3 %.

List of symbols

C_a	Humid air capability (s^2/m^2)
C_m	Moisture storage capacity ($\text{kg}/(\text{kg Pa})$)
C_p	Heat capacity ($\text{J}/(\text{kg K})$)
h_c	Heat convective exchange coefficient ($\text{W}/(\text{m}^2 \text{K})$)
h_m	Mass convective exchange coefficient ($\text{kg}/(\text{m}^2 \text{s Pa})$)
h_l	Mass enthalpy of liquid water (J/kg)
j_a	Dry air flow density ($\text{kg}/(\text{m}^2 \text{s})$)
j_l	Liquid flow density ($\text{kg}/(\text{m}^2 \text{s})$)
j_m	Total moisture flow density ($\text{kg}/(\text{m}^2 \text{s})$)
j_q	Heat flow density ($\text{J}/(\text{m}^2 \text{s})$)
j_v	Water vapor flow density ($\text{kg}/(\text{m}^2 \text{s})$)
k_l	Liquid permeability ($\text{kg}/(\text{m s Pa})$)
k_l^*	Liquid water conductivity due to water vapor pressure gradient ($\text{kg}/(\text{m s Pa})$)
k_m	Total moisture permeability ($\text{kg}/(\text{m s Pa})$)
k_v	Water vapor permeability ($\text{kg}/(\text{m s Pa})$)
k_p	Total moisture infiltration ($\text{kg}/(\text{m s Pa})$)
k_{pv}	Water vapor infiltration ($\text{kg}/(\text{m s Pa})$)
k_{pl}	Liquid infiltration ($\text{kg}/(\text{m s Pa})$)
k_T	Non-isothermal moisture transfer due to a thermal gradient ($\text{kg}/(\text{m s K})$)
L_v	Latent heat of vaporization (J/kg)
M	Liquid molar mass (kg/mol)
P	Total pressure (Pa)
P_c	Capillary pressure (Pa)
P_v	Water vapor pressure (Pa)
$P_{v,sat}$	Saturated vapor pressure (Pa)
R	Ideal gas constant ($\text{J}/\text{mol K}$)
S_l	Water saturation degree (–)
T	Temperature (K)
t	Time (s)
u_a	Dry air content (kg/m^3)
u_g	Gas content (kg/m^3)

✉ M. Y. Ferroukhi
mohammed_yacine.ferroukhi@univ-lr.fr

¹ LaSIE, UMR 7356 CNRS University of La Rochelle, Avenue Michel Crépeau, 17042 La Rochelle cedex1, France

² LMT-Cachan/ENS Cachan/CNRS/Université Paris Saclay, 61 Avenue du Président Wilson, 94230 Cachan, France

Greek letters

φ	Relative humidity (%)
σ	Ratio between water vapor exchange mass and the overall mass exchange (–)
α	Heat convection coefficients due to a water vapor pressure gradient (m^2/s)
γ	Heat convection coefficients due to a total pressure gradient (m^2/s)
λ	Thermal conductivity ($\text{W}/(\text{m K})$)
λ^*	Corrected thermal conductivity ($\text{W}/(\text{m K})$)
ω	Moisture content (kg/kg)
ε	Porosity (–)
ρ_e	Water density (kg/m^3)
ρ_g	Gas density (kg/m^3)
ρ_s	Dry density (kg/m^3)

Subscripts

i	Layer position in the wall from the outside to inside
m	Layer interface position
n	Layer position
x	Space
ext	External ambience
int	Internal ambience
ini	Initial condition
l	Left side of layer
r	Right side of layer

1 Introduction

Generally, buildings are exposed to various solicitations including external perturbations (solar radiation, rainfall and temperature) or internal ones (different heating and ventilation systems). All these solicitations are responsible of complex interactions of different heat and moisture transport mechanisms that occur simultaneously within the building envelope elements. The nature of these transfers is related to the properties of the studied materials that can induce specific phenomena such as: evaporation/condensation, sorption/desorption and hysteresis. Assuming all these coupled phenomena increases the complexity of the theoretical and experimental study.

Till now, various approaches for modeling the coupled heat, air and moisture (HAM) transfer through porous building's envelope are available in literature [1–7]; we can classify them according to the used driving potentials. Concerning the thermal transfer, the conventional driving source is temperature gradient. In contrast, for the moisture transfer there is no unanimity regarding the driving potentials choice. According to Funk [8], these models give fairly similar results, as there are, under specific assumptions laws that liaise between the various transfer motors as the ideal gas law and the Kelvin law [9].

Among these approaches there may be mentioned the model of Richards [10] who was among the first researcher to predict the water transport in partially saturated porous media. Although Darcy equation was originally designed for flows in saturated media, it was extended by the author to flow in the unsaturated zone, by providing that the constant of proportionality, called hydraulic conductivity, is function of the water content.

Further, Philip and De Vries [11] expressed the water content and the temperature as transfer drivers expressing the moisture transfer in a gradients of humidity and temperature. The energy equation is described only by heat transfer caused by molecular conduction and that associated with the phase change.

Later, Milly [12] developed the Philip and De Vries model by adding the hysteresis phenomenon of the retention curve. This has been achieved by considering the dependencies capillary potential and temperature, where liquid water is considered incompressible. The independent variable to describe the water status of the system used by Milly is the capillary potential. Adopting the same approach in deriving heat and moisture transfer equations for building materials, Pederson [13], decomposed the hydric transfer in two original transport equations taking vapor pressure and suction pressure as driving potentials for the vapor and liquid phase, respectively.

One year after, Lewis and Ferguson [14] confirmed the possibility of incorporating the total pressure as a complementary driving potential to the heat and mass transfer as expected initially by the Luikov study [15]. This pressure gradient generates an additional transport term resulting from the filtration motion of the liquid and vapor within the porous material. More specifically, air pressure can transport significant amounts of moisture that can be deposited on the wall surfaces leading to interstitial condensation or dramatically lack of control of temperature and relative humidity.

In this context, Dos Santos and Mendes [16] have developed a mathematical model to predict the transfer in a block of brick hollow, vapor transfer is by diffusion/convection and liquid flow is governed by Darcy's law. Recently, Remki et al. [7] evaluated the impact of atmospheric pressure gradient on the hygrothermal transfers in porous material by adding the total pressure effect in the mathematical model of heat, air and moisture transfers.

As such, most of these studies were applied on one monolayer wall contrary to the real application where the building envelope is assembled by a number of layers that separate the indoors from the outdoors environment. Among the few works on these multilayered materials, a dynamic multilayer model was developed by Qin et al. [17] where experimental approaches have been considered. Tests validation concern especially mortar and sandstone. Qin et al.

[17] chosen the vapor content as the principle driving potential for the moisture transfer as expected by Nilsson [18]; the role of the total pressure and convection were not considered in their study.

Otherwise, Bai et al. [19] adopts the Representative Elementary Volume method in deriving the combined transfer model in the multilayer non gray porous fibrous insulation. In fact, they numerically investigate whether natural convection can be ignored as a mode of heat transfer in high-porosity. Justly, they revealed that natural convection is more likely to occur when the heated/cooled rate is low, while natural convection can be ignored in simulating steady-state coupled heat transfer in multilayer insulation. It is preferable if these authors extend their study on other multilayered materials and not only the thermal insulation.

Later study shows an inverse analysis of heat transfer across a multilayer composite wall with Cauchy boundary conditions [20]. However, they consider one typical dynamic heat transfer problem where the role of moisture migration and convection were not considered. Likewise, in a recent study, Dias [21] interested on one transfer process which is the diffusion of heat.

Considering the problems of coupled HAM transfer through multilayer materials, the biggest difference between the monolayer and multilayer models is the choice of the moisture driving potential. The moisture content is discontinuous at the interface between two porous media, due to their different hygroscopic behavior. Complicated additional equations at the inner boundary are needed if moisture content is chosen as the driving potential for the multilayer case. Therefore, it is important to use a continuous parameter as the moisture driving potential.

To overcome this; the current paper addresses the question of HAM transfer in the case of representative multilayer building wall by exposing a detailed model and to define the validity of the sub model. This model consider the temperature as a driving potential for heat transfer, the total pressure for air transfer and the water vapor pressure for hydric transfer. The choice of the water vapor pressure as mass driving source is especially adapted on the model application that treat multilayer walls. This allows us to avoid the discontinuity problems at the wall layers interfaces, which is not the case with the water content. Moreover, the water vapor pressure is in direct relation with the relative humidity which is a useful parameter with a simple and direct signification, particularly when using experimentation. Based on this model, a numerical simulation is carried out and focuses on one-dimensional case. Further, new experimental procedure for measuring the moisture content and the temperature profiles within the materials has been investigated. This allows performing comparisons between the numerical and experimental results. All the hygrothermal properties of the tested

multilayered materials have been experimentally evaluated by adopting reliable characterization protocols.

2 Mathematical modeling

Predicting HAM transfer through multilayer envelope in accurate representative conditions of the building's environment is the main objective of the present work.

The proposed HAM transfer model is mainly inspired from [7, 15, 17] models, where the water vapor pressure is chosen as the principal driving potential for the moisture transfer and the role of the total pressure and convection are considered. Moreover, the developed model is applicable for both hygroscopic and non-hygroscopic materials that can be combined in different multilayer wall.

For the porous element domain the following assumptions are made in model:

- A local thermodynamic equilibrium between all present phases;
- The gaseous phase obeys the ideal gas law;
- The hysteresis and the chemical reaction between phases are not taken into account;
- Heat transfer by radiation are neglected;
- Variation of moisture storage power depending on temperature is neglected;
- Undeformable solid medium;
- Only mass of liquid and vapor are considered;
- Each layer of material is considered homogenous;
- The Dufour effect is neglected.

2.1 Governing equation

At first, the masse and energy balance equations are written for all considered phases (liquid, vapor and air) expressed as follows:

$$\frac{\partial u}{\partial t} = -\text{div}(j_l + j_v) \quad (1)$$

$$\frac{\partial u_a}{\partial t} = -\text{div}(j_a) \quad (2)$$

$$C_p \rho_s \frac{\partial T}{\partial t} = -\text{div}(j_q) \quad (3)$$

where, u, u_a (kg/m^3) are the total water content (vapor and liquid) and dry air content, j_l, j_v, j_a [$\text{kg}/(\text{m}^2 \text{ s})$] represent respectively, the mass flow density of the liquid, water vapor and dry air phases, j_q [$\text{J}/(\text{m}^2 \text{ s})$] is the heat flow density, t (s) time, T (K) temperature, C_p [$\text{J}/(\text{kg K})$] heat capacity, ρ_s (kg/m^3) dry density.

Then, the equations are defined according to the driving forces of transfer as it is presented in the following section.

2.1.1 Multi-phase moisture transfer equations

In unsaturated porous materials, moisture transfer occurs in two forms: liquid and vapor. The liquid transfer is mainly induced by suction pressure gradient obtained by direct application of Darcy's [first term of Eq. (4)], whereas the water vapor transport is considered as diffusional process governed by Fick's law, under a vapor pressure gradient [first term of Eq. (5)].

$$j_l = -k_l \nabla P_c - k_{pl} \nabla P \quad (4)$$

$$j_v = -k_v \nabla P_v - k_{pv} \nabla P \quad (5)$$

For both liquid and vapor flux [Eqs. (4, 5)], the contribution of vapor and liquid infiltration due to the total pressure gradient is well considered as expressed in the last term of each flux expression. This contribution was demonstrated by Luikov [15] and further developed by Remki et al. [7].

Whereas, the adopted mass flux expression includes both diffusive and convective contributions simultaneously, either for total or capillary pressures represented by Darcy's transfer; this leads to the following new expression of the total mass flux resulting from the addition of the liquid and vapor flux:

$$j_m = j_l + j_v = -k_l \nabla P_c - k_v \nabla P_v - k_p \nabla P \quad (6)$$

P_c : capillary pressure (Pa), P_v : water vapor pressure (Pa), k_l : liquid permeability [kg/(m s Pa)], k_v : water vapor permeability [kg/(m s Pa)], $k_p = k_{pv} + k_{pl}$: total moisture infiltration [kg/(m s Pa)], k_{pl} [kg/(m s Pa)] and k_{pv} [kg/(m s Pa)] are the infiltration coefficient corresponding to the liquid and the vapor phase, respectively.

Often by recasting physical laws in one driving potential, a very useful moisture transfer expression and physical phenomena quantification can be achieved. Therefore, kelvin law $P_c = \frac{RT\rho_e}{M} \ln\left(\frac{P_v}{P_{v,sat}}\right)$, is used for expressing the capillary pressure gradient as a combination of vapor pressure gradient and a temperature gradient. The temperature gradient appears in the ∇P_c equation because of the saturated vapor pressure that is function of temperature:

$$\nabla P_c = \left[\frac{RT\rho_e}{M} \frac{1}{P_v} \right] \nabla P_v + \left[\frac{RT\rho_e}{M} \left(\frac{\partial \ln\left(\frac{P_v}{P_{v,sat}}\right)}{\partial T} \right) + \frac{R\rho_e}{M} \ln\left(\frac{P_v}{P_{v,sat}}\right) \right] \nabla T \quad (7)$$

where; M : liquid molar mass (kg/mol), R : ideal gas constant [J/(mol K)], ρ_e : water density (kg/m³), $P_{v,sat}$: saturated vapor pressure (Pa) $p_{v,sat} = \exp\left(23,5771 - \frac{4042.9}{T-37.38}\right)$

By integrating Eq. (6) into (7), Eq. (8) is obtained:

$$j_m = -(k_l^* + k_v) \nabla P_v - k_T \nabla T - k_f \nabla P \quad (8)$$

with: $k_l^* = k_l \cdot \frac{RT\rho_e}{M} \cdot \frac{1}{P_v}$ represents the liquid water conductivity due to water vapor pressure gradient, expressed in [kg/(m s Pa)].

$$k_T = k_l \left(\frac{RT\rho_e}{M} \left(\frac{\partial \ln\left(\frac{P_v}{P_{v,sat}}\right)}{\partial T} \right) + \frac{R\rho_e}{M} \ln\left(\frac{P_v}{P_{v,sat}}\right) \right) \text{ expressed}$$

in [kg/(m s K)] is non-isothermal moisture transfer due to a thermal gradient. This last term is not a diffusion consequence of the temperature gradient; it represents a diffusional parasite term due to the choice of the driving potential (the transition from P_c to P_v) [22].

Thus, the phenomenological description consists in writing the equations according to driving forces of transfer described by: the total pressure, the temperature, and the humidity and the total mass density will be expressed as:

$$j_m = -k_m \nabla P_v - k_T \nabla T - k_p \nabla P \quad (9)$$

here, $k_m = k_v + k_l^*$ [kg/(m s Pa)], is the total moisture permeability.

Finally, the mass balance equation takes the following expression:

$$C_m \rho_s \frac{\partial P_v}{\partial t} = \text{div}(k_m \nabla P_v + k_T \nabla T + k_p \nabla P) \quad (10)$$

with, C_m represents the moisture storage capacity expressed as $(1/P_{v,sat}) \cdot (\partial \omega / \partial \varphi) \left[\frac{\text{kg}}{\text{kg Pa}} \right]$.

2.1.2 Dry air and water vapor transfer

In addition to the liquid and the water vapor transfers, moist and dry air transfer occurs, within the porous material by infiltration process [15]. More specifically, air can transport significant amounts of moisture that can be deposited on the wall surfaces leading to interstitial condensation or dramatically lack of control of temperature and relative humidity.

Using the same procedure of Remki et al. [7], this infiltration is governed by a total pressure gradient, as following:

$$j_a + j_v = -k_p \nabla P \quad (11)$$

Here, in Eq. (11) the presence of a gradient of total pressure within the material causes transfer of vapor and drying air simultaneously according to the infiltration type.

In the other hand, to get the air balance equation, the vapor and dry air contents are combined:

$$u_g = u_v + u_a = \varepsilon \frac{\rho_g}{\rho_s} (1 - S_l), \quad \rho_g = PM/RT \quad (12)$$

By combining Eqs. (11) and (12), Eq. (13) is obtained:

$$u_g = \varepsilon \frac{\rho_g}{\rho_s} (1 - S_l) = \frac{PM}{\rho_s RT} \varepsilon (1 - S_l) \tag{13}$$

ε : Porosity (–), S_l : water saturation degree (–)

Proceeding by a partial diversion of the Eq. (11):

$$d\left(\frac{PM}{\rho_s RT} \varepsilon (1 - S_l)\right) = \left(\frac{M}{\rho_s RT} \varepsilon (1 - S_l)\right) dP \tag{14}$$

By introducing Eq. (14) in the gaseous phase balance Eq. [7]:

$$C_a \frac{\partial P}{\partial t} = \text{div}(k_p \nabla P) \tag{15}$$

with $C_a = \frac{M}{\rho_s RT} \varepsilon (1 - S_l)$ expressed in (s²/m²).

2.1.3 Heat transfer

the thermal transfer in porous media occurs by conduction under a temperature gradient (Fourier law), by convection through the liquid and vapor flows and by a latent heat of phase change. Thereby, the heat flow density can be expressed as follows [7]:

$$j_q = -\lambda \nabla T + h_l j_m + L_v j_v \tag{16}$$

λ : thermal conductivity [W/(m K)], h_l : the mass enthalpy of liquid water (J/kg), L_v : latent heat of vaporization (J/kg).

By introducing the Eq. (9) into Eq. (16), the final of the heat flux density is obtained:

$$j_q = -(\lambda + h_l \cdot k_T) \nabla T - h_l (k_m \nabla P_v + k_p \nabla P) + L_v j_v \tag{17}$$

From Eqs. (3) and (17), the energy conservation equation is becomes:

$$C_p \rho_s \frac{\partial T}{\partial t} = \text{div}(\lambda^* \nabla T + \alpha \nabla P_v + \gamma \nabla P) + L_v C_m \sigma \frac{\partial P_v}{\partial t} \tag{18}$$

with: $\lambda^* = \lambda + h_l k_T$, $\alpha = h_l k_m$, $\gamma = h_l k_p$, $\sigma = \frac{\text{div}(j_v)}{\text{div}(j_m)}$.

The obtained Eqs. 10, 15 and 18 represent the coupled HAM transfer in monolayer porous building materials. It is a three driving potential system composed of water vapor pressure, total pressure for respectively humid and gaseous phases and temperature for heat:

While the continuity condition between layers is respected for the obtained system; this tater can be applied on a multilayer wall using the same techniques as Qin et al. [17]. Hens, the equations of the coupled heat, air and moisture transfer for multilayer walls with three driving potentials.

Water vapor pressure, total pressure for respectively humid and gaseous phases, temperature for heat is expressed as follows:

$$\begin{cases} C_{m_i}(\omega) \rho_{s_i} \frac{\partial P_v}{\partial t} = \text{div}(k_{m_i}(\omega) \nabla P_v + k_{T_i} \nabla T + k_{p_i} \nabla P) \\ C_{a_i} \frac{\partial P}{\partial t} = \text{div}(k_{p_i} \nabla P) \\ C_{p_i} \rho_{s_i} \frac{\partial T}{\partial t} = \text{div}(\lambda_i^*(\omega) \nabla T + \alpha_i \nabla P_v + \gamma_i \nabla P) + L_v \rho_{s_i} \sigma_i C_{m_i}(\omega) \frac{\partial P_v}{\partial t} \end{cases} \tag{19}$$

with “i” represents the layer position in the multilayer wall.

2.2 Initial and boundary conditions

The physical system is modeled as a multilayer porous wall with impermeable and adiabatic horizontal boundaries. The vertical conditions are kept at different temperature moisture and pressure that express exchange in building. The boundary justification of these conditions, at both wall sides in direct contact with ambiances is complex to define. This must ensure the coupling between the microscopic quantities defined within material and the macroscopic one of the external flow.

In the present study, convective heat and mass exchanges, related to the internal and external environmental excitations, are taken into consideration [Eqs. (20) and (21)]. Concerning the total pressure, Dirichlet boundary conditions are imposed [Eq. (21)].

According to the above analysis, these boundary conditions are summarized in the following equation from $x = 0$ to $x = n$:

$$k_{m_{0,n}}(\omega) \nabla P_v + k_{T_{0,n}} \nabla T + k_{f_{0,n}} \nabla P = h_{m_{ext,int}} (P_{v_{ext,int}} - P_v) \tag{20}$$

$$\begin{aligned} \lambda_{0,n} \nabla T + \alpha_{0,n} \nabla P_v + \gamma_{0,n} \nabla P &= h_{c_{ext,int}} (T_{ext,int} - T) \\ &+ (1 - \sigma) L_v h_{m_{ext,int}} (P_{v_{ext,int}} - P_v) \end{aligned} \tag{21}$$

$$P_0 = P_{ext} \quad \text{and} \quad P_n = P_{int} \tag{22}$$

Indices “int” and “ext” are the internal and external wall conditions.

Equation (20) represents the moisture balance at the surfaces ($x = 0$ and $x = n$); the three terms on the left-hand side describe the supply of moisture flux under the influence of a moisture gradient, a temperature gradient and a total pressure gradient respectively. The terms to the right side describe the amount of moisture drawn off from or into the surfaces and governed principally by convection. Equation (21) expresses the heat flux in terms of convection heat transfer at the surfaces ($x = 0$ and $x = n$).

The coefficients of mass and heat transfer by convection depend of several parameters (including the air flow condition, temperature, building geometry...), which makes them complex determination. In this study, the convective heat transfer coefficient determined by Schaube and Werner [23] is used. Whereas, the convective mass transfer coefficient is deduced from the heat transfer coefficient by

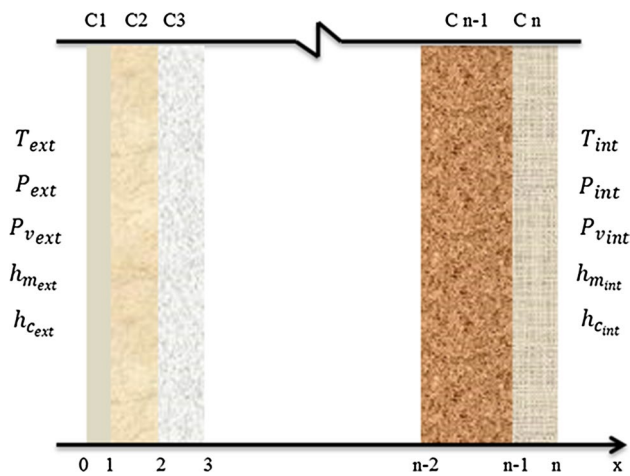


Fig. 1 General scheme of a multilayer wall

convection by considering the Illig analogy [24] approved experimentally by Schwarz [25].

Concerning the interfaces contact between wall layers; the boundary conditions are taken into account as follows: For $x = 1, 2, \dots, n - 1$:

$$P_{v_{m_l}} = P_{v_{m+1_r}}, \quad T_{m_l} = T_{m+1_r}, \quad P_{m_l} = P_{m+1_r}, \quad m = 1, 2, \dots, n \quad (23)$$

where, “l” and “r” indices respectively represent left and right interfaces of layer “m” (Fig. 1).

Initial conditions are fixed in the wall for $t = 0$:

$$P_v(x, 0) = P_{v_{ini}}, \quad P(x, 0) = P_{ini}, \quad T(x, 0) = T_{ini} \quad (24)$$

3 Experimental investigation

As expected previously, there is a need for more experimental data that predict the real behavior of multilayered materials representing of real building configuration; therefore a new experimental setups adapted to these materials tests has been developed in the present work. This part is also devoted to validate the real behavior of the developed HAM transfer model in multilayers configuration case.

The experimental validation was conducted by controlling relative humidity and temperature profiles for a steady state situation. That is why, four samples composed of two different materials (insulation besides a wall component type) each one, referring to the real wall composition have been investigated.

The tested materials are: red brick, chipboard, plaster and expanded polystyrene. So these manufactured samples represent four types of multilayer walls configurations. The samples thicknesses were taken enough small to optimize the test time, given the hygrothermal transfer kinetics and especially the water transfer which is relatively slow. The

Table 1 Tested samples thicknesses

Sample	Configuration
1	Red brick (3 cm) + expanded polystyrene (1 cm)
2	Red brick (3 cm) + plaster (1 cm)
3	Chipboard (3 cm) + plaster (1 cm)
4	Chipboard (3 cm) + expanded polystyrene (1 cm)

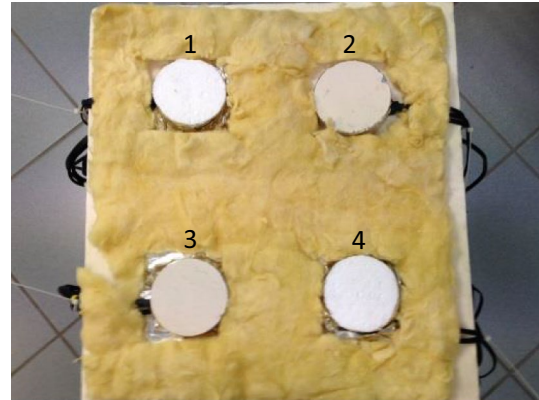


Fig. 2 Samples insulation

samples diameter is 8 cm. The tested samples and their corresponding thicknesses are summarized in Table 1.

The samples were isolated laterally to foster unidirectional hygrothermal transfer (Fig. 2).

The test principle consists on submitting samples to two hygrothermal controlled environments. The temperature is maintained for each ambiance with a thermostatic bath who feeds a copper heat exchanger. For the relative humidity control, saturated salt solutions were used. Figure 3 illustrates the experimental device in initial configuration without insulation; later both ambiances were well covered in order to ensure the stability of the imposed boundary conditions.

All the samples were submitted to a constants temperature and relative humidity gradients with conditioning the upper compartment at a temperature of 17 °C and relative humidity of 65 %. For the inferior compartment, the temperature was fixed at 33 °C and 35 % of relative humidity. These selected gradients are so representatives of the building environments conditions.

It should be noted that during the experiment tests, the temperature and the relative humidity average variations at the two compartments was respectively of 0.5 °C and 1.4 %, which is acceptable.

For monitoring the temperature and the relative humidity profiles along the sample during the test, hygrothermal sensors were implemented at different thickness of the

Fig. 3 Experimental device

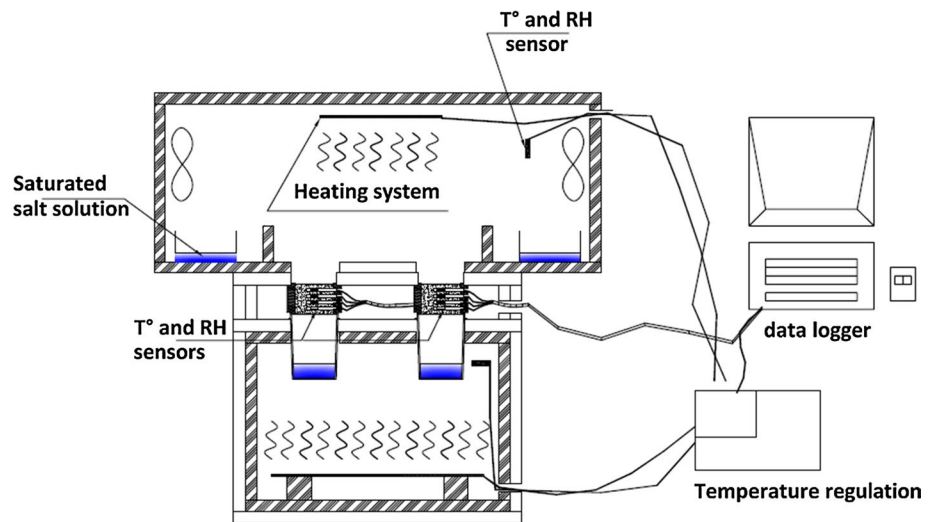


Fig. 4 Sensors locations in the samples

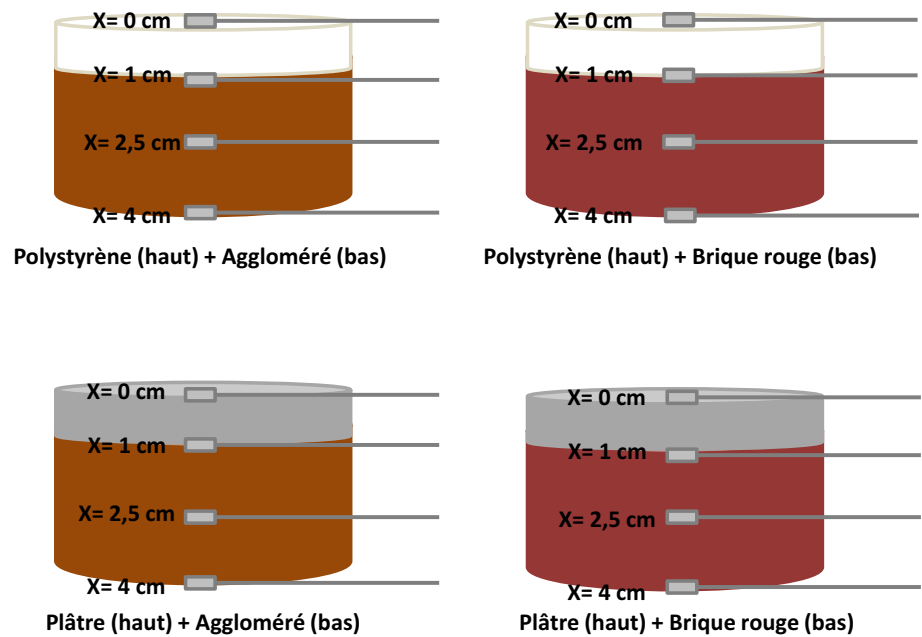


Fig. 5 Sensirion data logger and SHT75 sensor

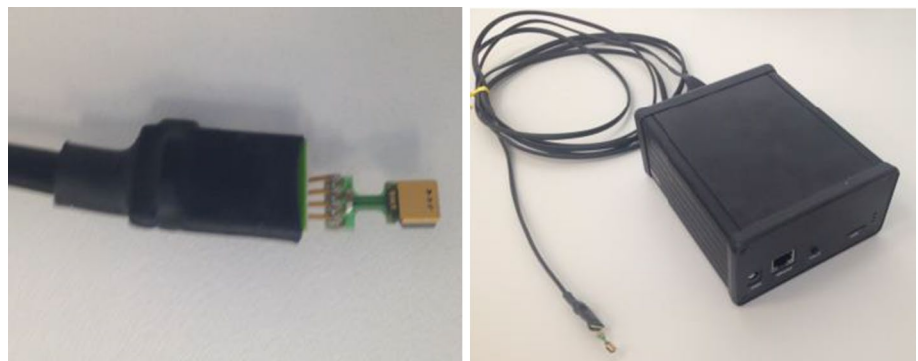


Table 2 Technical characteristics of SHT75 sensor

Technical characteristics	
Relative humidity precision	1.8 %
Temperature precision	0.3 °C
Maximum resolution	8 s
RH measurement range	0 to 100 % HR
Temperature measurement range	−40 to 125 °C

samples. These sensors are connected directly to a data logger unit that can record, the temperature and relative humidity profiles of the tested samples for low steps time (5 min). Figures 4 and 5 represent the data logger type and the used sensors and their location in the samples.

Regarding the dimension of the multilayered samples it is important that the sensors do not affect the hygrothermal behavior. That is why, the sensors used in this experiment (SHT75 sensors) are suited for this application [6, 17, 26], as their small size (depth of 3 mm and width of 5 mm). provides a stable and reliable measurement. Technical characteristics of SHT75 sensor are summarized in Table 2.

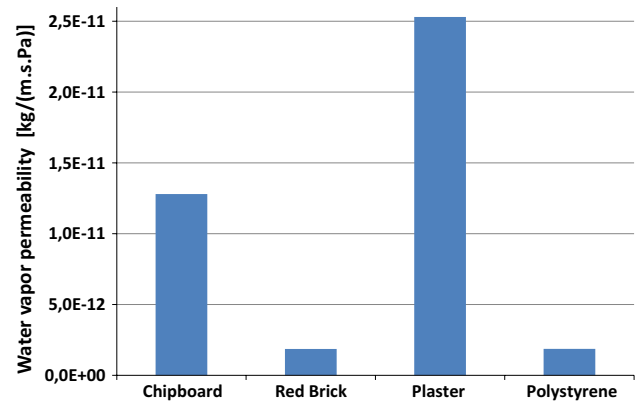
3.1 Hygrothermal characterization for the numerical simulation

In order to examine the numerical hygrothermal behavior of the tested multilayered configurations, an estimation of the input parameters of the developed HAM model is required. In fact, one of the difficulties with the use of this model lies to the refine identification of these parameters characterizing the hygrothermal materials properties. That is way; a part of the present work was devoted to the evaluation of the main properties of materials through the development of various experimental prototypes in the laboratory. The interest is to have a reliable prediction and to better reproduce numerically the hygrothermal behavior of samples.

Initially, the water vapor permeability has been evaluated among the selected properties. This parameter was determined using the Gravitest (GINITRONIC, Suisse) equipment based on the cup method according to the European Standard EN ISO 12572. The experimental procedure consists to make a regular monitoring, until equilibrium, of sample mass subjected to a water vapor pressure gradient under isothermal conditions (23 °C) [27].

In this case, water vapor pressure gradient was created by imposing relative humidity of 50 and 95 % between the two faces of the tested sample. Obtained water vapor permeabilities are represented in Fig. 6.

Similarly, another parameter has been determined; it is the water storage capacity of materials. This parameter was

**Fig. 6** Water vapor permeability of tested materials

calculated from the adsorption and desorption isotherm curves of water vapor evaluated using the BELSORP-Aqua3 equipment. The device in question operates with a volumetric method which consists of defining the adsorbed gas quantity by the sample until reaching a steady state. This measure allows subsequently calculate the sample water content at each pressure level [28]. Figure 7 represents adsorption–desorption curves of materials used in the experimental validation. From these results, it can be seen that the Chipboard present a very high storage capacity compared to the red brick witch illustrate, seriously, the necessity to take this parameter in consideration during modelling.

Another hygrothermal parameter that should be evaluated and presents an important heat sensitivity generally observed between insulations and other ordinary materials is the thermal conductivity. It was achieved by using the Lambda-meter Ep 5000e. The test tool operates with the guarded hot plate apparatus method according to ISO 8302 DIN EN 1946-2 DIN EN 12667 and ASTM C177 (DIN 52612) norms.

Lambda-Meter EP500e measures the sample thickness (e (m)) and its area (A (m²)), the temperature deference over the sample (ΔT (K)) well as the unidirectional heat flux (Q (W)) thought the sample. Then, thermal conductivity is determined: $\lambda = \frac{Q \cdot e}{\Delta T \cdot A}$

Results for materials used in the experimental validation are shown in Fig. 8 and obtained at 23 °C.

Concerning the specific heat capacity evaluation the DSC (Differential Scanning Calorimetry) method under a nitrogen flow of 50 ml/min is required.

The technique consists to determine the absorbed or liberated heat flow variation from the material by measuring the temperature in a controlled atmosphere. The specific heats obtained for each used material are summarized in Fig. 9.

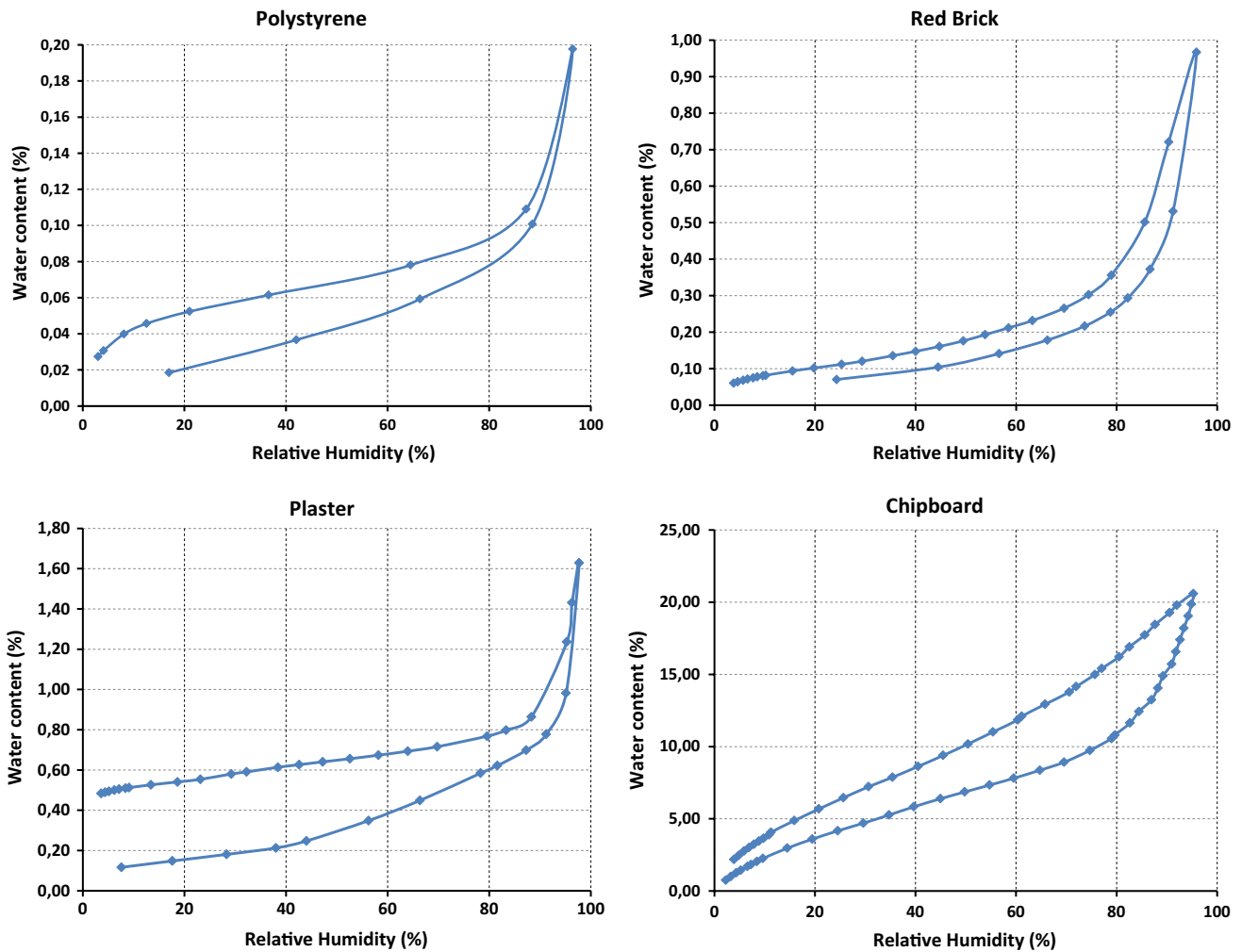


Fig. 7 Adsorption and desorption isotherm curves

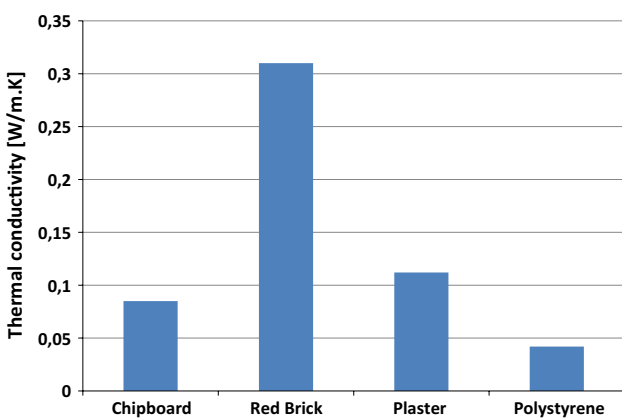


Fig. 8 Thermal conductivity of tested materials

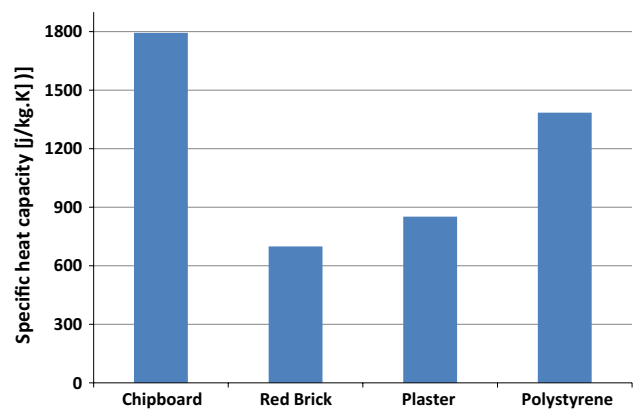


Fig. 9 Specific heat capacity of tested materials

The results of the experimental characterization conducted in the above part were used as input parameters of the HAM model developed in the Sect. 2. Table 3

summarizes the thermal and hydric properties of the tested materials in the experimental validation the developed hygrothermal transfer model.

Table 3 Hygrothermal properties of tested materials

Property	Chipboard	Red brick	Plaster	Polystyrene
ρ_s [kg/m ³]	562	1670	1353	20.4
C_p [J/(kg K)]	1794	699	852	1385
λ [W/(m K)]	0.085	0.310	0.112	0.042
k_m [kg/(m s Pa)]	1.28×10^{-11}	1.86×10^{-12}	2.53×10^{-11}	1.87×10^{-12}

It is noted that to perform the numerical simulation task, evidently, the initial and boundary conditions are identical to those of the experiment.

4 Numerical simulation and validation

The numerical simulations were realized on COMSOL Multiphysics software [29], which is particularly suitable for treating several phenomena simultaneously, as is the case for coupled heat, air, and moisture transfer. Also, the assessment of the HAM transfers on other phenomena such as the ingress of aggressive agents (chlorides, carbonation) and the ingress of pollutants (Volatile Organic Compounds) becomes possible. In our study, this software is used particularly for solving partial differential equations using Finite Element (FE) method. Various kind of meshes are easily generated which is more convenient for 3D studies. COMSOL PDE solving presents great assortment of FE algorithms: (UMFPACK, GMRES, Multi-grid.) [29]. In the present study it concerns the UMFPACK solver. It solves general systems of the form $Ax = b$ using the nonsymmetric-pattern multifrontal method and direct LU factorization of the sparse matrix A where solution is established by applying the Quadratic-Lagrange method. More detailed applications of the FEM for solving heat transfer problems are done by Minkowycs et al. [30].

In the current application, the numerical solution appears as temperatures and vapor content profiles within the multilayer wall allowing possibility of comparison with the hygrothermal profiles obtained experimentally. It is to notice that the simulation is based on the boundary conditions used in the experiments, so the radiation is not considered here.

The numerical and experimental comparison of temperature and water vapor pressure distributions in the multilayer studied configurations are shown in Figs. 10, 11, 12 and 13. This distribution was done function of 3 time series where the selected top time is 15 days which correspond to the steady state period. Contrarily to Qin et al. [17] this steady state is rapidly obtained because of the small selected thicknesses and the high material porosity. The sensors positions are shown in Fig. 4 where the insulation layer is less thick than the material for the same multilayered composition. The hygrothermal profiles are done for

each sensors position. Continuous lines correspond to the numerical results while the points represent the experimental one.

The average difference between measured and predicted results was expressed by a root-mean-square error [31]. The average errors δ_{RMS} for each configuration are shown in the figures titles's. Generally, these values fit the experimental data very well (the small value is about 0.27 %).

In Figs. 10b, 11, 12 and 13b, the heat transfer kinetics is fast, where the steady state is reached only after a 100 h while for the hydric transfer (Figs. 10a, 11, 12, 13a) steady's state is reached more slowly. Also, the temperature

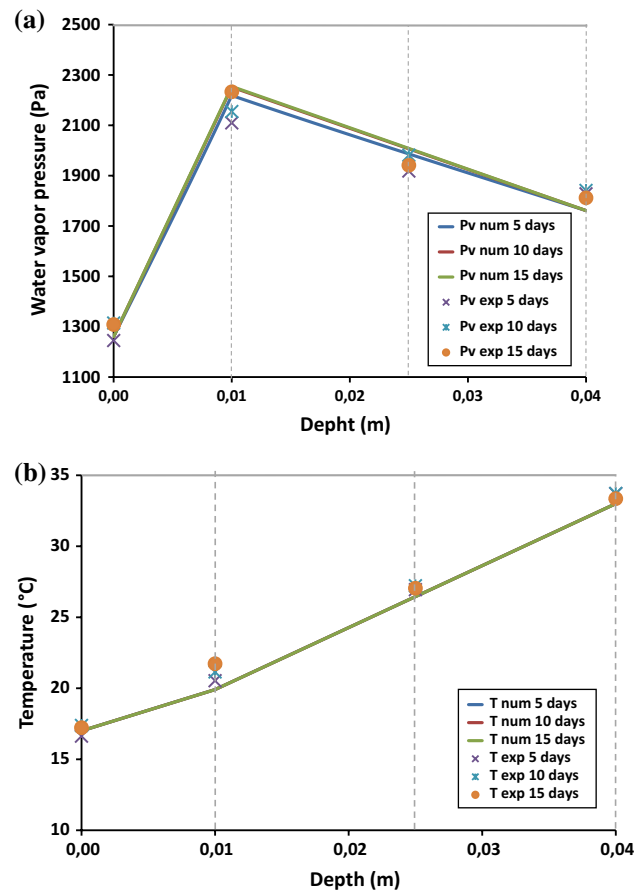


Fig. 10 Comparison of computed distribution with experimental data for configuration 1 (red brick + plaster). **a** Water vapor pressure distribution ($\delta_{RMS} = 4.99$ %). **b** Temperature distribution ($\delta_{RMS} = 0.30$ %)

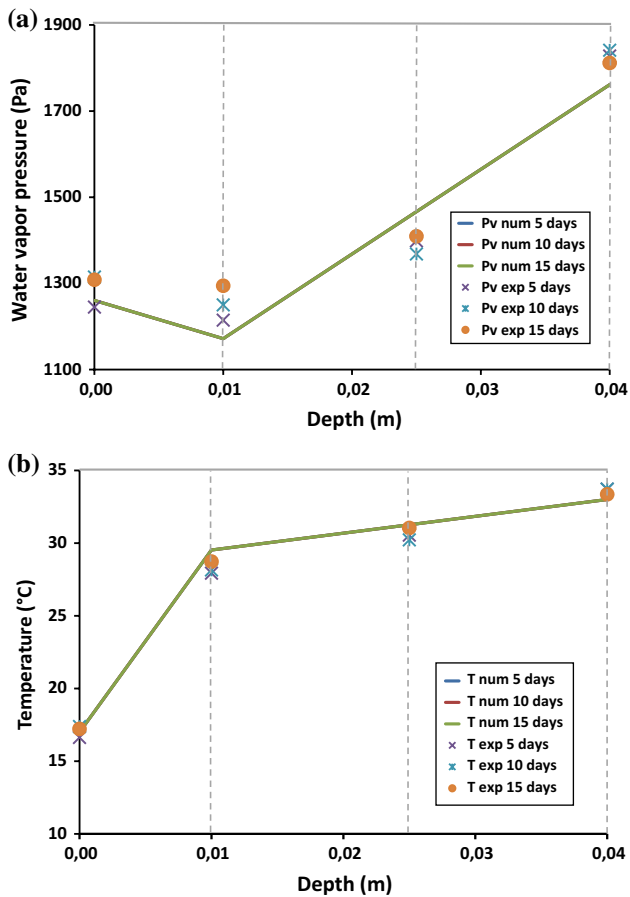


Fig. 11 Comparison of computed distribution with experimental data for configuration 2 (red brick + polystyrene). **a** Water vapor pressure distribution ($\delta_{RMS} = 4.91\%$). **b** Temperature distribution ($\delta_{RMS} = 0.27\%$)

and vapor pressure profiles change shape for the four studied configurations because of their different nature and storage capacity.

For example, the two multilayered combination red brick-plaster and red brick-polystyrene present completely different distributions; plaster promotes absorbing vapor content as it is hygroscopic which explain the high value of vapor pressure (Fig. 10a distribution between 0 and 0.01 m). Indeed, within the red brick-plaster couple, a high competition of the moisture adsorption between the plaster and red brick is produced because they have the same hygroscopicity level (as obtained by the sorption desorption isotherm in Fig. 7). Furthermore, plaster present a very high permeability (as obtained in Fig. 6) compared to the red brick which confirm this water migration to the brick (in Fig. 10).

However, in red brick-polystyrene combination (Fig. 11a) polystyrene behaves as moisture bridge; this result can be justified by its very low vapor adsorption (it adsorb a maximum of 0.2 % whereas the brick adsorb a

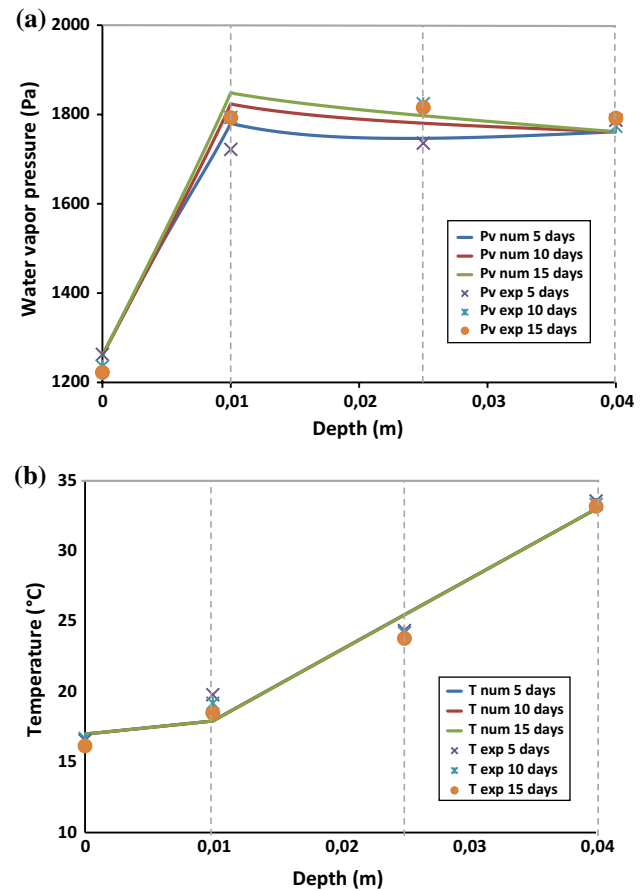


Fig. 12 Comparison of computed distribution with experimental data for configuration 3 (chipboard + plaster). **a** Water vapor pressure distribution ($\delta_{RMS} = 2.09\%$). **b** Temperature distribution ($\delta_{RMS} = 0.34\%$)

maximum of 1 % as shown in Fig. 7). Brick and polystyrene have almost the same vapor permeability (Fig. 6); this favors the moisture transport to the red brick and reduces the discontinuity problem between the two layers composition. By consequence, the thermal performance of this insulation material can be degraded because of this hydric migration; as it can be observed on the slight temperature increase on the right side of (Fig. 11b).

In other manner, if we compare the plaster behavior in the two couples (plaster-red brick and plaster chipboard) in Figs. 10 and 12 respectively; a big similitude of the temperature and vapor pressure profiles is obtained. Indeed, it can be seen that the plaster behaves as a good insulator against the thermal solicitations because of the slight observed temperature variation within this material (Figs. 10b, 12b). By contrast, this material is still faithful to its hygroscopic properties since it lets moisture transported either to the brick or the chipboard; which is confirmed by the vapor pressure drop (from $x = 0$ to $x = 0.01$ m) in Figs. 10a and 12a. This is naturally justified

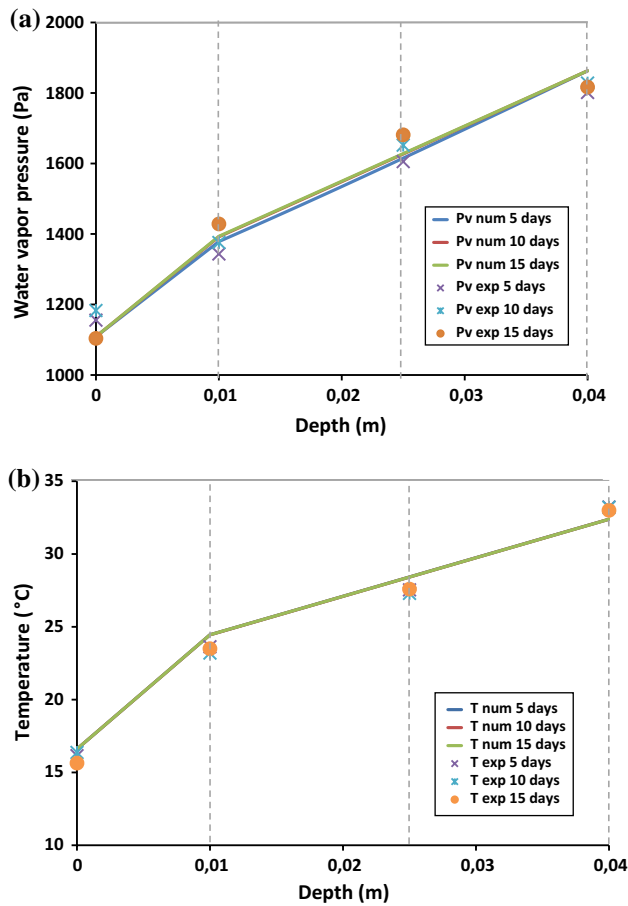


Fig. 13 Comparison of computed distribution with experimental data for configuration 4 (chipboard + polystyrene). **a** Water vapor pressure distribution ($\delta_{RMS} = 2.98\%$). **b** Temperature distribution ($\delta_{RMS} = 0.28\%$)

by its highest vapor permeability compared to the other materials (Fig. 6). Concerning the moisture adsorption theoretically the chipboard adsorb moisture more than the red brick implying higher water content measurement in the plaster-chipboard combination. In reality the measured vapor pressure values in this material combination was not so high which suggests that the permeability of material has a considerable influence on the moisture transfer as expected above.

Concerning the polystyrene combinations comparison (polystyrene-red brick and polystyrene chipboard) shown in Figs. 11 and 13 respectively, thermally similar temperature responses can be noted; the temperature slop within the polystyrene is higher than those obtained for plaster. Regarding the vapor pressure profiles (Figs. 11a, 13a), polystyrene left vapor migration without any adsorption or increase in moisture content inside as explained above. But in the layer contact polystyrene the higher vapor pressure was measured for the polystyrene chipboard since the chipboard is well recognized by its high hygroscopicity

compared to the red brick. (As it is indicated in the sorption desorption isotherms above in Fig. 7).

Further, by comparing the obtained experimental results with performed simulations, there is a good agreement between the temperature and water vapor pressure profiles for the four studied configurations. This correlation is illustrated by the low average errors between the numerical and experimental data, where there is a maximum error of $\delta_{RMS} = 0.34\%$ (Chipboard + plaster) for temperature profiles. For water vapor pressure profiles, the errors are relatively large, with a maximum error of $\delta_{RMS} = 4.91\%$ (Red brick + polystyrene). These errors can send it either, of experimental process, particularly the sensors implementation at the material itself or at the interface between two different materials, which can disrupt their hygrothermal behavior. Another source of errors is the input data for hygrothermal transfer model. A small input data variation leads to a modification of the hygrothermal behavior prediction of the material [32].

5 Conclusion

In this work, a coupled heat, air and moisture transfer model in multilayer walls was developed and examined. This model is based on driving potentials that ensure continuity at the interfaces between layer walls. Selected driving potentials are a state variables (water vapor pressure, total pressure and temperature), which are not dependent on the solid support of material or morphology of its pore space. On the other hand, the proposed model of hygrothermal behavior prediction in the wall is based on simple input parameters.

Further, an experimental device was designed to study the hygrothermal behavior of several configurations of multilayer porous building materials. Heat and moisture transfer evolutions in the samples were monitored over time, as well as good control of boundary conditions. In this context, an experimental characterization of the tested constituent materials was completed. In particular, evaluation of adsorption–desorption curves, water vapor permeability, thermal conductivity and specific heat were performed.

Comparison of temperature and water vapor pressure profiles resulting from the numerical simulation with those obtained experimentally for the four tested configurations were undertaken. The results showed good agreement between predicted and measured data. These good results illustrate the advantages of the proposed hygrothermal transfer model, with accessible input data, evaluable experimentally with standardized tests.

This study reveals that the plaster behaves like a water vapor sponge reducing the incoming moisture flow and good insulation. Centrally, the polystyrene behaves as

bridge transporting the water to the hygroscopic material which causes lack of control on temperature and degradation of the thermal performance of this insulation material.

Acknowledgments This work was funded by the French National Research Agency (ANR) through the Program Sustainable Cities and Buildings (Project HUMIBATex n°ANR-11-BVD).

References

- Häupl P, Grunewald J, Fechner H (1997) Coupled heat air and moisture transfer in building structures. *Int J Heat Mass Transf* 40(7):1633–1642
- Hagentoft C (2002) HAMSTAD final report: methodology of HAM-modeling, report R-02:8, Gothenburg, Department of Building Physics, Chalmers University of technology, Sweden
- Mendes N, Philippi PC (2005) A method for predicting heat and moisture transfer through multilayered walls based on temperature and moisture content gradients. *Int J Heat Mass Transf* 48(1):37–51
- Grunewald J, Nicola A (2006) BES manual. <http://beel.syr.edu/champs.htm>
- Woloszyn M, Rode C (2007) IEA Annex 41, MOIST-ENG Subtask 1—modelling principles and common exercises, final report
- Belarbi R, Qin M, Ait mokhtar A, Nilsson LO (2008) Experimental and theoretical investigation of non-isothermal transfer in hygroscopic building materials. *Build Environ* 43:2154–2162
- Remki B, Abahri K, Tahlaoui M, Belarbi R (2012) Hygrothermal transfer in wood drying under the atmospheric pressure gradient. *Int J Therm Sci* 57:135–141
- Funk M, Wakili KG (2007) Driving potentials of heat and mass transport in porous building materials: a comparison between general linear, thermodynamic and micromechanical derivation schemes. *Transp Porous Media* 72:273–294
- Daïan JF (2013) ÉQUILIBRE ET TRANSFERTS EN MILIEUX POREUX. I- Etat d'équilibre. p:183 <hal-00452876v1> France
- Richards L (1931) Capillary conduction of liquids through porous mediums. *Physics* 1(5):318–333
- Philip J, De Vries D (1957) Moisture movement in porous material under temperature gradients. *Trans Am Geophys Union* 2:222–232
- Milly P, Christopher D (1982) Moisture and heat transport in hysteretic, inhomogeneous porous media: a matrix head-based formulation and a numerical model. *Water Resour Res* 18(3):489–498
- Pedersen CR (1992) Prediction of moisture transfer in building constructions. *Build Environ* 27:387–397
- Lewis R, Ferguson W (1993) A partially nonlinear finite element analysis of heat and mass transfer in a capillary-porous body under the influence of a pressure gradient. *Appl Math Model* 17(1):15–24
- Luikov AV (1966) Heat and mass transfer in capillary porous bodies. Pergamon, London
- Dos Santos GH, Mendes N (2009) Heat, air and moisture transfer through hollow porous blocks. *Int J Heat Mass Transf* 52:2390–2398
- Qin M, Belarbi R (2005) Development of an analytical method for simultaneous heat and moisture transfer in building materials utilising transfer function method. *J Mater Civil Eng ASCE* 5(17):492–497
- Nilsson LO (2003) Moisture mechanics in building materials and building components. Ph.D. thesis, Lund Institute of Technology, Sweden
- Bai D, Fan XJ (2007) On the combined heat transfer in the multilayer non-gray porous fibrous insulation. *J Quant Spectrosc Radiat Transf* 104(3):326–341
- Niu RP, Liu GR, Li M (2014) Inverse analysis of heat transfer across a multilayer composite wall with Cauchy boundary conditions. *Int J Heat Mass Transf* 79:727–735
- Dias CJ (2015) A method of recursive images to solve transient heat diffusion in multilayer materials. *Int J Heat Mass Transf* 85:1075–1083
- Janssen H (2011) Thermal diffusion of water vapour in porous materials: fact or fiction? *Int J Heat Mass Transf* 54:1548–1562
- Schaube H, Werner H (1986) Heat transfer coefficient under natural climatic conditions. *IBP-Mitt.* 13 Nr 109
- Illig W (1952) The magnitude of the water vapor transfer value during diffusion processes in walls of housing units, stables and cold storage rooms. *Gesund Ing* 73(7/8):124–127
- Schwarz B (1971) Heat and material transfer in outdoor wall surfaces. Diss.Universität Stuttgart, Stuttgart
- Ruut P, Rode C (2004) Common Exercise 1 – Case 0A and 0B Revised, IEA, Annex 41, Task 1, Modeling Common Exercise
- Issaadi N, Nouviaire A, Belarbi R, Ait-Mokhtar A (2014) Etude comparative des techniques d'arrêt d'hydratation et de leurs conséquences sur les propriétés de transfert hydrique des matériaux cimentaires, France
- Abahri K (2012) Modeling of coupled heat, air and moisture transfer in porous building materials ». La Rochelle university, La Rochelle
- FEMLAB AG (2007) FEMLAB AG, Comsol 33 Multiphysics FEM Software package
- Minkowycs W, Sparrow E, Murthy J (2006) Handbook of numerical heat transfer, 2nd edn. Wiley, USA
- Zarr RR, Burch DM, Fannery AH (1995) Heat and moisture transfer in wood-based wall construction: measured versus predicted. *NIST Build Sci Ser* 173:83
- Ferroukhi MY, Belarbi R, Limam K (2014) Effect of hygrothermal transfer on multilayer walls behavior, assessment of condensation risk. *Adv Mater Res* 1051:647–655